



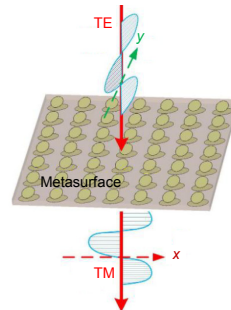
DOI: 10.12086/oee.2020.190052

# Extraordinary strong optical rotation in weak chiral metasurface

Cui Jianhua<sup>1,2</sup>, Ma Xiaoliang<sup>1</sup>, Pu Mingbo<sup>1</sup>,Guo Yinghui<sup>1</sup>, Luo Xiangang<sup>1\*</sup>

<sup>1</sup>State Key Laboratory of Optical Technologies on Nano-Fabrication and Micro-Engineering, Institute of Optics and Electronics, Chinese Academy of Science, Chengdu, Sichuan 610209, China;

<sup>2</sup>University of Chinese Academy of Science, Beijing 100049, China



**Abstract:** A preternatural and extremely thin metasurface with weak asymmetric unit structure is presented here to demonstrate extraordinary strong chirality. The unit cell of metasurface is composed of a double layer of elliptical metal patches with a certain twisted angle and a medium sandwiched between them. When the twisted angle equals to 80°, optical activity can be realized in this metasurface. At the resonant frequency 11.89 GHz, the incident linearly polarized wave is converted into its cross-polarization wave with the transmittance rate higher than 94%. The light weight and miniaturization of this metasurface provide a reliable approach for polarization manipulation. If extended to light waveband, the metasurface may have potentials in biological applications such as detection of weak chiral molecules, etc.

**Keywords:** metasurface; chirality; extraordinary; optical activity

**Citation:** Cui J H, Ma X L, Pu M B, et al. Extraordinary strong optical rotation in weak chiral metasurface[J]. *Opto-Electronic Engineering*, 2020, 47(7): 190052

## 弱手性超表面中的超常极化旋转

崔建华<sup>1,2</sup>, 马晓亮<sup>1</sup>, 蒲明博<sup>1</sup>, 郭迎辉<sup>1</sup>, 罗先刚<sup>1\*</sup>

<sup>1</sup>中国科学院光电技术研究所微细加工光学技术国家重点实验室, 四川 成都 610209;

<sup>2</sup>中国科学院大学, 北京 100049

**摘要:** 本文介绍了一种能够产生超强旋光性的弱手性极薄( $\lambda/10$ )亚波长结构的超表面。该超表面的单元结构由介质层以及设置在介质层上下表面的两层椭圆金属贴片组成, 两层椭圆金属贴片之间存在一个扭转角的关系。当扭转角为 80° 时, 超表面在谐振频点 11.89 GHz 处能将入射线偏振电磁波转换为交叉极化透射波, 其透过率超过 94%。这种超表面重量轻、体积小, 为极化旋转提供了一种可靠的方法。若将其拓展到光波波段, 该超表面在弱手性分子的生物学检测中有潜在的应用。

**关键词:** 超表面; 手性; 超常; 旋光性

---

收稿日期: 2019-01-29; 收到修改稿日期: 2019-08-06

基金项目: 国家自然科学基金资助项目(61622508, 61622509)

作者简介: 崔建华(1980-), 女, 博士研究生, 助理研究员, 主要从事亚波长光学的研究。E-mail: sklotm@126.com

通信作者: 罗先刚(1970-), 男, 博士, 研究员, 主要从事微纳光学的研究。E-mail: lxg@ioe.ac.cn

版权所有©2020 中国科学院光电技术研究所

中图分类号: TB33

引用格式: 崔建华, 马晓亮, 蒲明博, 等. 弱手性超表面中的超常极化旋转[J]. 光电工程, 2020, 47(7): 190052

文献标志码: A

## 1 Introduction

As a special kind of material, chiral material refers to the material with basic unit cells that cannot superpose with their mirror images like human hands. Almost all natural organic molecules are chiral, such as DNA and protein molecules, sugar solution, etc. As there are no symmetric planes in chiral materials, the cross-coupling between the electric and magnetic fields exist. The cross-coupling between electric and magnetic waves results in peculiar electromagnetic performances such as circular dichroism (CD)<sup>[1]</sup> and optical rotation (OR)<sup>[2]</sup>. Unfortunately, the chirality of natural chiral material is rather weak and large thickness is needed to design useful applications, resulting in large weight and volume that is hard to integrate and minimize. In recent years, metamaterials have provided a new approach to solve the disadvantages and breakthrough the confinement in traditional materials. The electromagnetic properties of metamaterials are mainly determined by the basic artificial subwavelength unit cells, which are composed of multiple materials with certain arrangements and designed shapes. The artificial unit cells are the basic operating elements to modulate the amplitude and phase of the incident electromagnetic wave instead of the molecule of the composing materials. The artificial unit cell of metamaterials can greatly increase the strength of coupling with incident waves and breakthrough the confinement of traditional material. Some particular performances have been realized by metamaterials<sup>[3]</sup>, such as negative fraction index<sup>[4-7]</sup>, anti-Doppler effect<sup>[8-9]</sup>, perfect lens<sup>[4, 10]</sup>, etc.

Metasurfaces<sup>[11-12]</sup>, as its name implies, are the counterpart of planar metamaterials. Compared with traditional metamaterials, they are easier to realize in micro & nanofabrication technology. In chiral metasurfaces, the CD and OR characters have proved to be greatly strengthened to utilize with thinner thickness. Several types of chiral metasurface have been proposed to present giant artificial chirality based on their asymmetric unit cells, including gammadiion shapes<sup>[13-14]</sup>, twisted cross shape<sup>[15-16]</sup>, U-shape structures<sup>[17-18]</sup> and twisted metallic arcs<sup>[19-20]</sup>, etc. These chiral metasurfaces present amazing performance in polarization manipulating at dual or multiple frequency bands. In recent years, many chiral metasurfaces for cross-polarization rotation have been

reported, among which common structural forms include double-layer chiral metasurfaces structure<sup>[21-22]</sup>, double-layer anisotropic metasurfaces structure<sup>[23-24]</sup>, and tri-layer composite metasurfaces<sup>[25-26]</sup>. For the first structural form, the double-layer chiral metasurfaces are enantiomeric relations, and the chiral metasurface usually has the four-fold rotational symmetry, while the mirror symmetry is broken. For the second structural form, there is a 90° rotational symmetry relationship between the two-layer anisotropic structures, and the anisotropic structure is constructed by asymmetrically introducing slit in the isotropic structure. For the third structural form, it has three layers of subwavelength structure separated by dielectric slabs, and the structures of the top layer and the bottom layer are usually rotationally symmetrical at an angle of 90 degrees.

## 2 Design and simulation

Here we propose a new type chiral metasurface based on two layers of twisted elliptical structure. Comparing to the above mentioned chiral metasurfaces, this one appears rather weak chirality due to its almost symmetric structure. However, this weak chiral metasurface performs giant optical rotation at the operating frequency, which is that the incident linearly polarized wave is converted into its cross polarized wave with the transmittance rate higher than 94%. The simple structure of this metasurface is beyond common knowledge of chiral structures, and provides a new opportunity for high efficiency polarization manipulation.

The scheme unit cell of this chiral metasurface is shown in Fig. 1(a). The unit cell is composed of a double layer of elliptical metal patches with a certain twisted angle and a medium sandwiched between them. The relationship between two elliptical metal structures are not orthogonal, but there is a twisted angle  $\phi=90-2\theta=80^\circ$  ( $\theta=5^\circ$ ) around their normal axis in  $z$  direction. Therein  $\theta$  indicates the included angle between the long axis of the metallic elliptic and its adjacent coordinate axis. The periods of the unit cell in the  $x$  and  $y$  directions are both  $p=11$  mm, and the long axis of the elliptic is  $a=8.2$  mm while the short axis is  $b=4.9$  mm. The thickness of the metallic structure is 0.035 mm. The substrate in the unit cell is chosen as Preperm L900HF, whose permittivity is 9

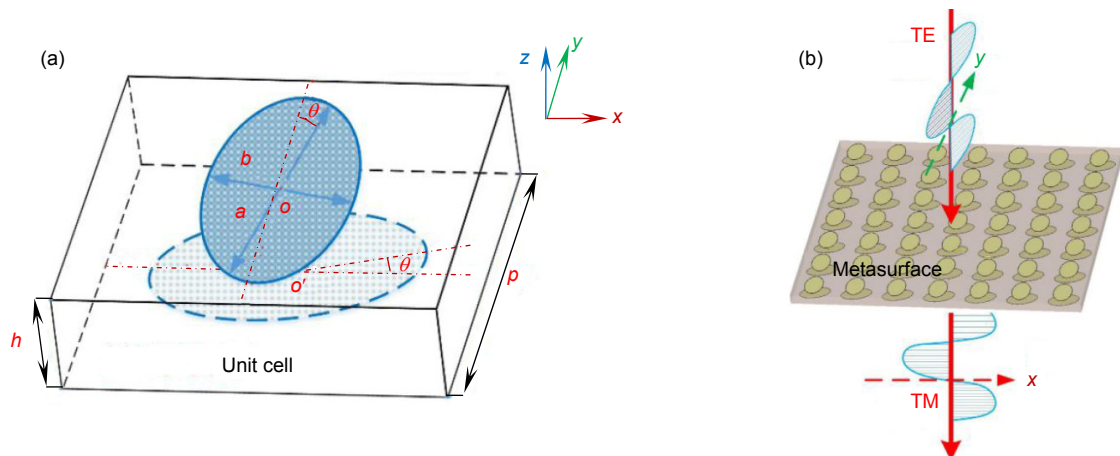


Fig. 1 (a) The unit cell of the proposed polarization rotator with weak chirality;  
(b) Operating principle diagram of the polarization rotator

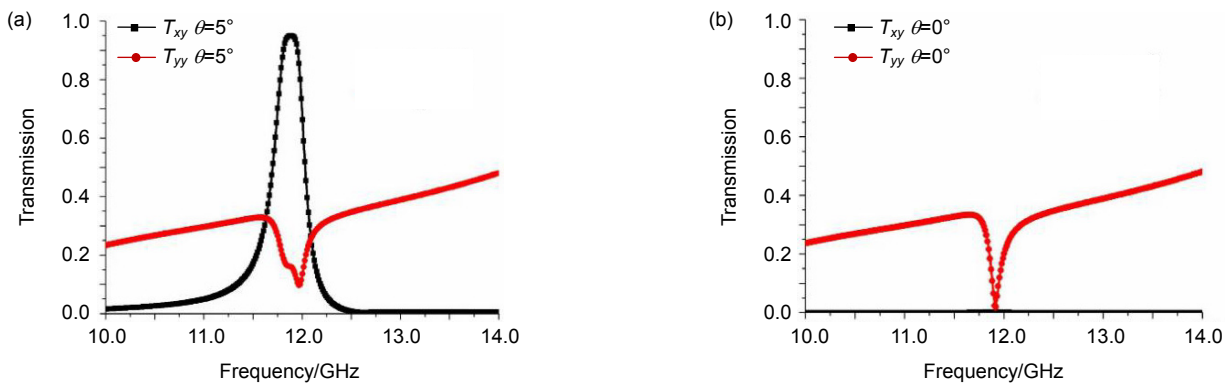


Fig. 2 The transmission curves of the proposed unit cell when  $\theta$  equals to  $5^\circ$  (a) and  $0^\circ$  (b)

and the loss tangent is 0.0004. The thickness of the substrate is  $h=2.8$  mm. It can be clearly seen that when the twisted angle  $\phi$  between the two long axes of upper and bottom metallic elliptic equals to  $90^\circ$ , the total unit is isotropic. Fig. 1(b) shows the operating principle diagram of the polarization rotator. When the  $y$ -axis polarized electromagnetic wave is incident on the chiral metasurface,  $x$ -axis polarized electromagnetic wave in the direction is produced. It can also be said that the TE wave is converted to a TM wave after polarization conversion.

The chiral metasurface was simulated by the commercial software CST Microwave Studio. With  $y$ -polarized incident microwave, the transmissions of both the  $x$ - and  $y$ -polarization were calculated, as shown in Fig. 2. It can be seen that the  $x$ -polarized component of the transmitted wave is much higher than  $y$ -polarized component at 11.89 GHz. The transmission rate  $T_{xy}$  reaches 94.6%, which clearly demonstrates that the incident  $y$ -polarized wave has been converted into  $x$ -polarized wave by this chiral metasurface. The polarization conversion efficiency can be calculated using the formula:

$$R = \frac{|T_{xy}|^2 - |T_{yy}|^2}{|T_{xy}|^2 + |T_{yy}|^2},$$

and the corresponding result is 94.6% at the operating resonance.

As comparison, we also simulated the co- and cross-polarization transmission of the isotropic unit with  $\phi=90^\circ$ , and the spectra are depicted in Fig. 2(b). It can be observed that when the twisted angle  $\phi$  equals to  $90^\circ$ , the transmission of the  $x$ - and  $y$ -polarized components are both close to 0 at the 11.89 GHz. The results prove that the unit cell is achiral and presents a giant reflective character in this situation. The comparison shows that the weak chirality in this metasurface indeed generates giant optical activity.

In order to reduce dielectric layer thickness and dielectric loss of the chiral metasurface, we choose microwave slab Preperm L900HF with high dielectric constant and low tangential loss. The affection of the dielectric parameters and thickness of the substrate on the polarization rotation phenomenon are studied. Fig. 3 provides the cross-polarization transmission of metasurface with

different dielectric parameters of the substrate. With the increase of dielectric constant, the center frequency of polarization rotation shifts to low frequency. Fig. 4 provides cross-polarization transmission of metasurface with different loss tangent of the substrate. As shown in the figure, the affection of tangent loss on the transmission is particularly obvious. When the loss tangent ( $\tan\delta$ ) is zero, the transmission of polarization rotation reaches 97%. When  $\tan\delta=0.0004$ , the transmittance rate reaches 94%; when  $\tan\delta=0.004$ , the transmission will be 75%; when  $\tan\delta=0.04$ , the transmission will drop sharply to 15%. Fig. 5 provides cross-polarization transmission curves of the chiral metasurface with different thicknesses  $h$  of the

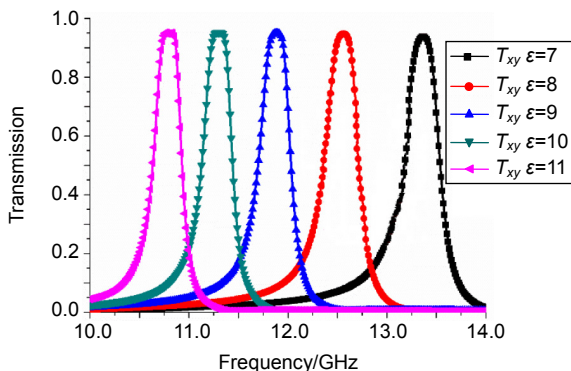


Fig. 3 Cross-polarization transmission curves vs. dielectric parameters of the substrate

dielectric layer. As shown in the picture, the center frequency of polarization rotation shifts to low frequency with the increase of dielectric layer thickness, but there is an optimum thickness when other structural parameters are fixed.

Subsequently, we analyzed the effect of the rotation angle of the chiral metasurface. The included angle  $\theta$  was varied with the step of  $1^\circ$  from  $0^\circ$  to  $7^\circ$ , and the transmission of  $x$ - and  $y$ -polarized components were calculated with  $y$ -polarized incidence, as shown in Figs. 6(a) and 6(b). It is presented that when  $\theta$  increases, the transmission of the cross-polarization increases first and then decreases when  $\theta$  is larger than  $5^\circ$  at the central frequency.

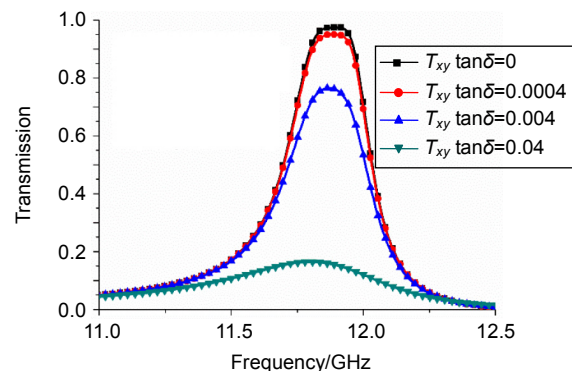


Fig. 4 Cross-polarization transmission curves vs. loss tangent of the substrate

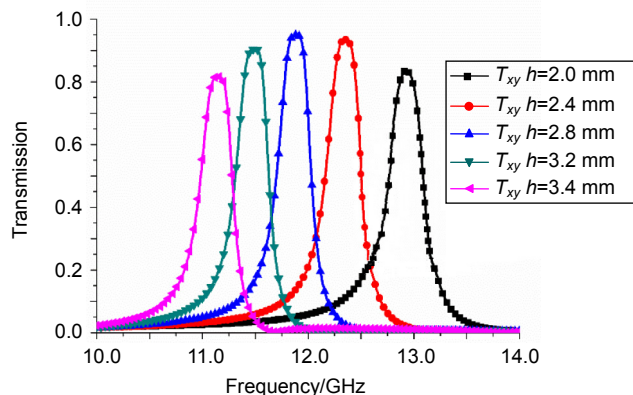


Fig. 5 Cross-polarization transmission curves vs. thicknesses of the substrate

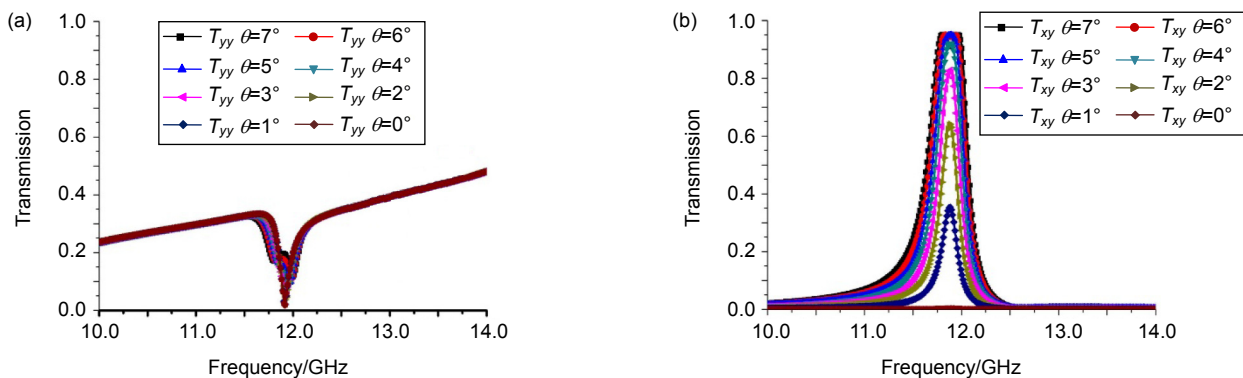


Fig. 6 The changing situation of the transmission with the unit cell at different little rotate angles

However, in the process of varying the rotation angle, the transmission of the co-polarization is almost unchanged, as depicted in Fig. 6(a).

The included angle  $\theta$  was then varied with the step of  $5^\circ$  from  $10^\circ$  to  $25^\circ$ , and the transmission of  $x$ - and  $y$ -polarized components were calculated with  $y$ -polarized incidence, as shown in Figs. 7(a) and 7(b). From these figures, we can see that the resonance peak of  $y$ -polarization transmission wave will split into two, when the rotation angle of chiral metasurface is larger than  $\theta=5^\circ$ , and the two split resonant peaks shift to both sides with the enlargement of the rotation angle.

### 3 Theoretical analyses

The chiral factors in the chiral subwavelength structure can be analyzed by observing the surface current of the subwavelength structure. When the structure of subwavelength element is anisotropic and chiral respectively ( $\theta=5^\circ$ ), the surface current distribution under the incidence of  $y$ -polarized electromagnetic waves is shown in Figs. 8(a) and 8(b). When the structure of subwavelength element is isotropic ( $\theta=0^\circ$ ), the surface current distribu-

tion under is shown in Fig. 8(c). It can be seen that the isotropic subwavelength structure generates symmetrical surface current distribution when the  $y$ -polarized electromagnetic wave is incident, so the superimposed field intensity of the induced electric field in the  $x$  direction is zero. In contrast, when the upper and lower elliptical sheet metal rotated reversely along its axis after  $5^\circ$ , due to the asymmetry of the structure and strong coupling between the layers,  $y$ -polarization of the incident electromagnetic wave in the subwavelength structure spark surface current distribution along  $x$  direction, and resulting the induced electric field along  $-x$  or  $+z$  direction at different instantaneous time, so as to realize the transformation of polarization. In other words, when the included angle is  $5^\circ$ , there are two main electromagnetic coupling modes on the metasurface. The resonance peaks of both modes coincide at 11.89 GHz.

As mentioned earlier, when the angle is large, the polarization rotation of the metasurface occurs at two frequency points. For instance, the surface current distribution of unit cells with the included angle  $\theta=15^\circ$  at frequencies of 11.60 GHz and 12.14 GHz are shown in Figs. 9(a) and 9(b) respectively under the incidence of

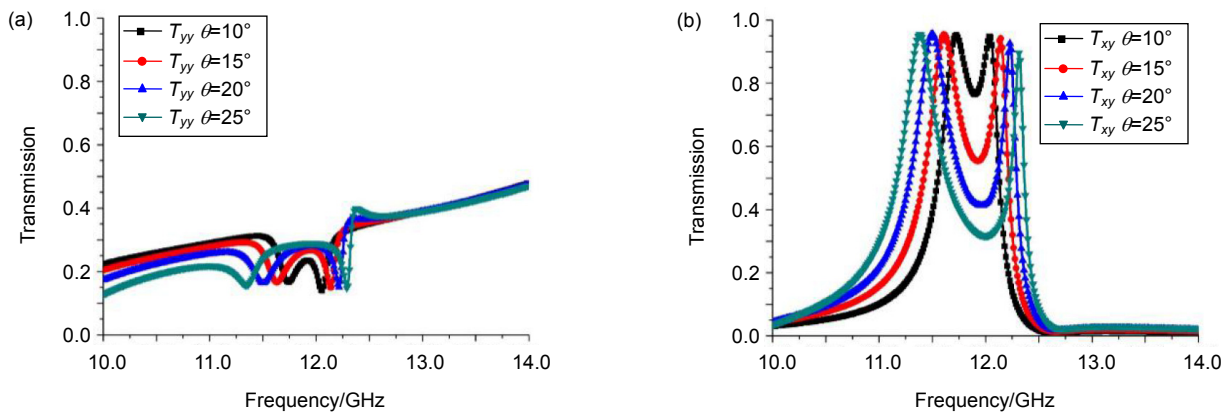


Fig. 7 The changing situation of the transmission with the unit cell at different large included angles

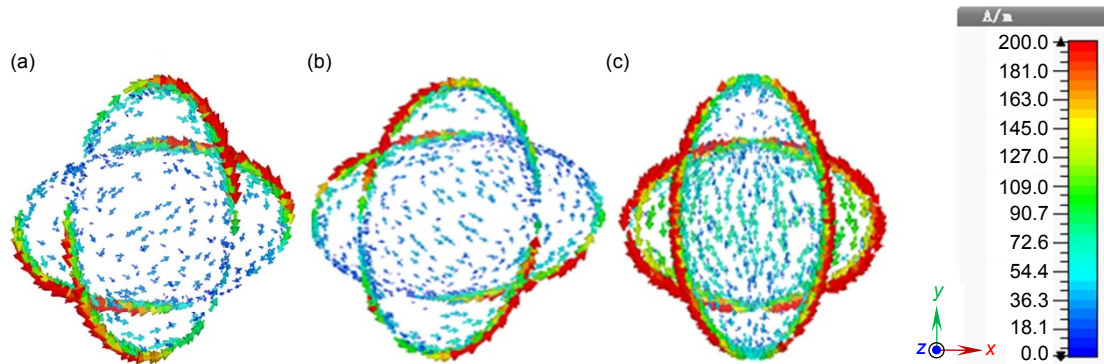


Fig. 8 The surface current distributions of unit cells with the included angle  $\theta=5^\circ$  ((a), (b)) and  $\theta=0^\circ$  (c)

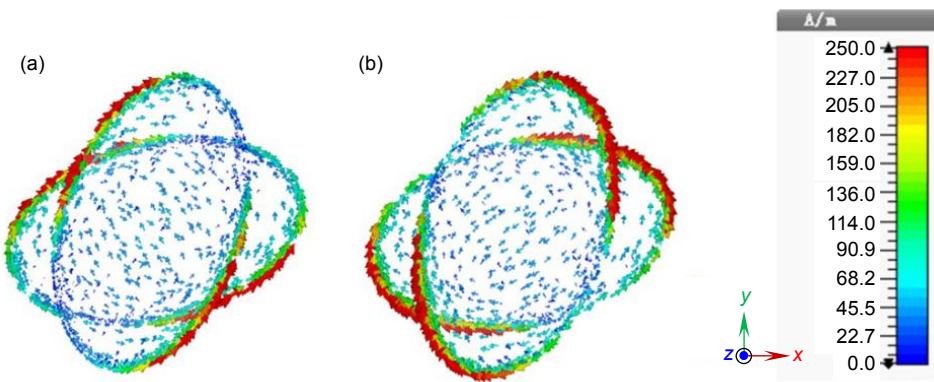


Fig. 9 The surface current distributions of unit cells with the included angle  $\theta=15^\circ$  at frequencies of 11.60 GHz (a) and 12.14 GHz (b)

$y$ -polarized electromagnetic waves. As shown in the figure, the induced electric field is along  $-x$  direction at 11.60 GHz and along  $+x$  direction at 12.14 GHz. Comparing with the surface current distributions at the included angle of  $5^\circ$ , it can be found that the obvious difference of structural parameters between the two main resonance modes increases at large angles, which makes the resonance occur at different frequencies.

The polarization conversion characteristics of electromagnetic wave can be described by polarization rotation angle and ellipticity. When the  $y$ -polarized wave enters vertically along the  $+z$  direction, the polarization rotation angle  $\Phi$  and ellipticity  $\eta$  can be defined as

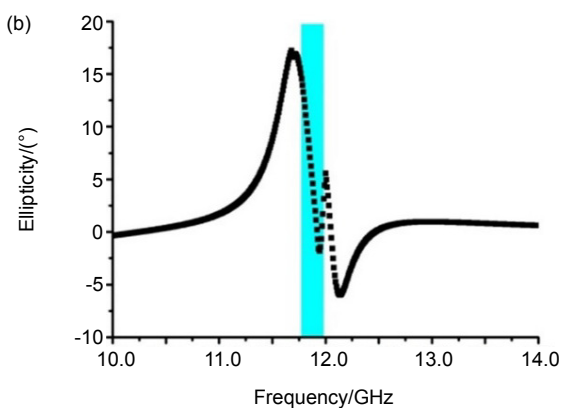
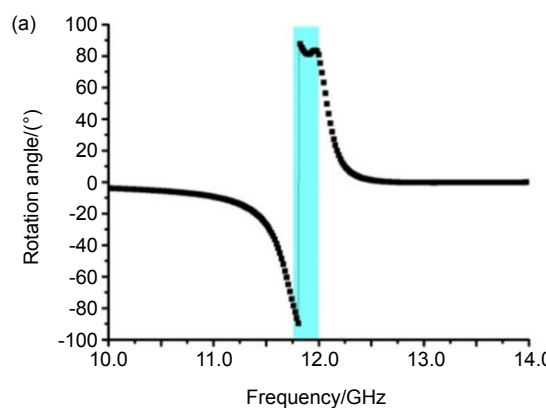
$$\Phi = \frac{1}{2} \arctan \left( \frac{2C \cos \varphi}{1 - C^2} \right), \quad (1)$$

$$\eta = \frac{1}{2} \arcsin \left( \frac{2C \sin \varphi}{1 + C^2} \right), \quad (2)$$

wherein,

$$C = \frac{|t_{xy}|}{|t_{yy}|}$$

and



$$\varphi = \arg(t_{xy}) - \arg(t_{yy}).$$

The polarization rotation angle represents the rotation angle of the electric field direction of the transmitted electromagnetic wave compared to the incident electromagnetic wave. Ellipticity represents the polarization state of transmission. When the  $\eta=0^\circ$ , the transmission of electromagnetic wave is proved to be linear polarization wave. Otherwise, the transmitted wave is in other forms of polarization of electromagnetic wave. Therefore, the conditions of polarization conversion from the  $y$  directional polarization into the  $x$  polarized wave are,  $\eta=0^\circ$  and  $\Phi=90^\circ$ . Fig. 10 shows polarization rotation angle of incidence and ellipticity for the  $y$  polarization normal incidence wave along the  $z$  direction with the rotation angle  $\theta=5^\circ$ . As shown from the simulation results, the polarization rotation angle is about  $81^\circ$  at 11.89 GHz which is close to  $90^\circ$ , ellipticity is about  $3.3^\circ$  at 11.89 GHz which is close to  $0^\circ$ . This means that the linearly polarized wave is converted to its orthogonal polarized wave, that is, the incident  $y$ -polarized wave is converted to the  $x$ -polarized wave.

Fig. 10 The simulated polarization rotation angle (a) and ellipticity (b) of the weak chiral metasurface

## 4 Conclusions

In summary, we present a preternatural chiral metasurface to demonstrate the extraordinary strong chirality from its weak asymmetric unit structure. The scheme unit cell of this chiral metasurface is composed of two layers of identical metallic elliptic, and the two elliptical structures are twisted by an angle of  $\phi=90-2\theta=80^\circ$  ( $\theta=5^\circ$ ) around their normal axis in  $z$  direction. Optical activity is realized in this metasurface and the incident linearly polarized wave is converted into its cross-polarization wave at the frequency of 11.89 GHz with the transmittance rate higher than 94%. And when the twisted angle of the two elliptical structures is reduced, two resonance peaks produced for optical rotation. The thickness of the metasurface is less than one tenth of the operating wavelength. The light weight and miniature of this metasurface provide a reliable approach for polarization manipulation. If extended to light waveband, the metasurface may have potentials in biological applications such as detection of weak chiral molecules etc.

## References

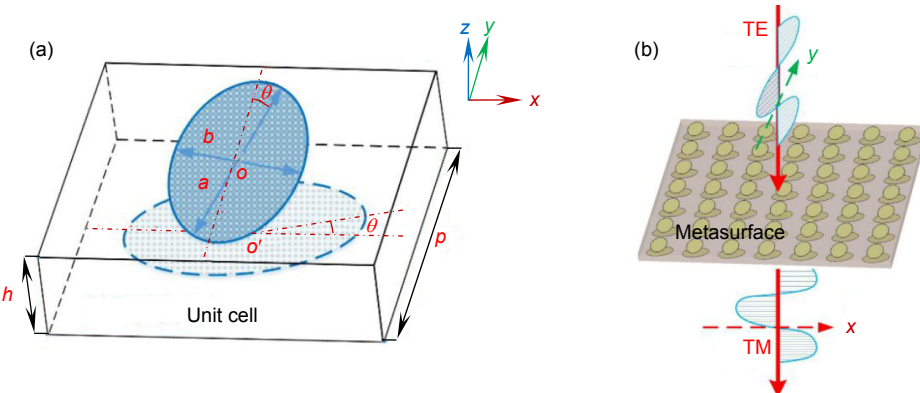
- [1] Cheng Y Z, Nie Y, Wu L, et al. Giant circular dichroism and negative refractive index of chiral metamaterial based on split-ring resonators[J]. *Physical Review Letters*, 2013, **110**(4): 421–432.
- [2] Zhang S, Park Y S, Li J, et al. Negative refractive index in chiral metamaterials[J]. *Physical Review Letters*, 2009, **102**(2): 023901.
- [3] Tian X Y, Yin L X, Li D C. Current situation and trend of fabrication technologies for three-dimensional metamaterials[J]. *Opto-Electronic Engineering*, 2017, **44**(1): 69–76.  
田小永, 尹丽仙, 李涤尘. 三维超材料制造技术现状与趋势[J]. 光电工程, 2017, **44**(1): 69–76.
- [4] Pendry J B, Holden A J, Stewart W J, et al. Extremely low frequency plasmons in metallic mesostructures[J]. *Physical Review Letters*, 1996, **76**(2): 4773–4776.
- [5] Cardano F, Marrucci L. Spin-orbit photonics[J]. *Nature Photonics*, 2015, **9**(12): 776–778.
- [6] Luo W J, Xiao S Y, He Q, et al. Photonic spin hall effect with nearly 100% efficiency[J]. *Advanced Optical Materials*, 2015, **3**(8): 1102–1108.
- [7] Diaz-Rubio A, Asadchy V S, Elsakka A, et al. From the generalized reflection law to the realization of perfect anomalous reflectors[J]. *Science Advance*, 2017, **3**(8): e1602714.
- [8] Chen J B, Wang Y, Jia B H, et al. Observation of the inverse Doppler effect in negative-index materials at optical frequencies[J]. *Nature Photonics*, 2011, **5**(4): 239–242.
- [9] Reed E J. Physical optics: backwards Doppler shifts[J]. *Nature Photonics*, 2011, **5**(4): 199–200.
- [10] Liu Y C, Ke Y G, Zhou J X, et al. Manipulating the spin-dependent splitting by geometric doppler effect[J]. *Optics Express*, 2015, **23**(13): 16682–16692.
- [11] Zhang Z J, Liang Y Z, Xu T. Research advances of hyperbolic metamaterials and metasurfaces[J]. *Opto-Electronic Engineering*, 2017, **44**(3): 276–288.  
张子洁, 梁瑜章, 徐挺. 双曲超材料及超表面研究进展[J]. 光电工程, 2017, **44**(3): 276–288.
- [12] Nemati A, Wang Q, Hong M H, et al. Tunable and reconfigurable metasurfaces and metadevices[J]. *Opto-Electronic Advances*, 2018, **1**(5): 180009.
- [13] Rogacheva A V, Fedotov V A, Schwanecke A S, et al. Giant gyrotropy due to electromagnetic-field coupling in a bilayered chiral structure[J]. *Physical Review Letters*, 2006, **97**(17): 177401.
- [14] Plum E, Zhou J, Dong J, et al. Metamaterial with negative index due to chirality[J]. *Physical Review B*, 2009, **79**(3): 035407.
- [15] Zhou J F, Dong J F, Wang B N, et al. Negative refractive index due to chirality[J]. *Physical Review B*, 2009, **79**: 121104.
- [16] Li Z F, Alici K B, Colak E, et al. Complementary chiral metamaterials with giant optical activity and negative refractive index[J]. *Applied Physics Letters*, 2011, **98**(16): 161907.
- [17] Gansel J K, Thiel M, Rill M S, et al. Gold helix photonic metamaterial as broadband circular polarizer[J]. *Science*, 2009, **325**(5947): 1513–1515.
- [18] Li Z F, Zhao R K, Koschny T, et al. Chiral metamaterials with negative refractive index based on four “U” split ring resonators[J]. *Applied Physics Letters*, 2010, **97**(8): 081901.
- [19] Ma X L, Huang C, Pu M B, et al. Multi-band circular polarizer using planar spiral metamaterial structure[J]. *Optics Express*, 2012, **20**(14): 16050–16058.
- [20] Ma X L, Huang C, Pu M B, et al. Dual-band asymmetry chiral metamaterial based on planar spiral structure[J]. *Applied Physics Letters*, 2012, **101**(16): 161901.
- [21] Song K, Liu Y H, Fu Q H, et al. 90° polarization rotator with rotation angle independent of substrate permittivity and incident angles using a composite chiral metamaterial[J]. *Optics Express*, 2013, **21**(6): 7439–7446.
- [22] Song K, Zhao X P, Liu Y H, et al. A frequency-tunable 90°-polarization rotation device using composite chiral metamaterials[J]. *Applied Physics Letters*, 2013, **103**(10): 101908.
- [23] Cheng Z Z, Cheng Y Z. A multi-functional polarization convertor based on chiral metamaterial for terahertz waves[J]. *Optics Communications*, 2019, **435**: 178–182.
- [24] Huang C, Ma X L, Pu M B, et al. Dual-band 90° polarization rotator using twisted split ring resonators array[J]. *Optics Communications*, 2013, **291**: 345–348.
- [25] Cong L Q, Cao W, Zhang X Q, et al. A perfect metamaterial polarization rotator[J]. *Applied Physics Letters*, 2013, **103**(17): 171107.
- [26] Mutlu M, Ozbay E. A transparent 90° polarization rotator by combining chirality and electromagnetic wave tunneling[J]. *Applied Physics Letters*, 2012, **100**(5): 051909.

# Extraordinary strong optical rotation in weak chiral metasurface

Cui Jianhua<sup>1,2</sup>, Ma Xiaoliang<sup>1</sup>, Pu Mingbo<sup>1</sup>, Guo Yinghui<sup>1</sup>, Luo Xiangang<sup>1\*</sup>

<sup>1</sup>State Key Laboratory of Optical Technologies on Nano-Fabrication and Micro-Engineering, Institute of Optics and Electronics, Chinese Academy of Science, Chengdu, Sichuan 610209, China;

<sup>2</sup>University of Chinese Academy of Science, Beijing 100049, China



(a) The unit cell of the proposed polarization rotator with weak chirality; (b) Operating principle diagram of the polarization rotator

**Overview:** A preternatural and extremely thin ( $\lambda/10$ ) metasurface with weak asymmetric unit structure is presented here to demonstrate extraordinary strong chirality. The unit cell of metasurface is composed of a double layer of elliptical metal patches with a certain twisted angle and a medium sandwiched between them. The relationship between two elliptical metal structures are not orthogonal, but there is a twisted angle  $\phi=90-2\theta=80^\circ$  ( $\theta=5^\circ$ ) around their normal axis in  $z$  direction. Therein  $\theta$  indicates the included angle between the long axis of the metallic elliptic and its adjacent coordinate axis. Optical activity is realized in this metasurface and the incident linearly polarized wave is converted into its cross-polarization wave at the resonant frequency with the cross-polarization transmittance rate higher than 94% at center frequency 11.89 GHz.

In addition, the polarization rotation characters of the metasurface under other different included angles  $\theta$  are studied. When the included angle  $\theta=0^\circ$ , the transmission of the  $x$ - and  $y$ -polarized components are both close to 0 at the 11.89 GHz, which proves that the unit cell is achiral and presents giant reflective character in this situation; when the included angle  $\theta$  varied with the step of  $5^\circ$  from  $10^\circ$  to  $25^\circ$ , the resonance peak of cross polarization transmission wave will split into two, and the two split resonant peaks shift to both sides with the enlargement of the rotation angle.

The chiral characters of the metasurface are studied by observing the surface current distributions of the subwavelength structure. When  $\theta=0^\circ$ , the subwavelength structure generates symmetrical surface current distribution, so the superimposed field intensity of the induced electric field in the  $x$  direction is zero. That is, the structure of subwavelength element is isotropic, and there is no chirality. When  $\theta=5^\circ$ , due to the asymmetry of the structure and strong coupling between the layers, the  $y$ -polarization of the incident electromagnetic wave in the subwavelength structure spark surface current distribution along  $x$  direction, so as to realize the transformation of polarization, which demonstrate extraordinary strong chirality. When  $\theta$  larger than  $10^\circ$ , the surface current distribution modes of unit cells generate corresponding to two different polarization rotation frequencies, which is demonstrate that there is double frequency chirality in the metasurface.

The light weight and miniaturization of this metasurface provide a reliable approach for polarization manipulation. If extended to light waveband, the chiral metasurface may have potentials in biological applications such as detection of weak chiral molecules etc.

**Citation:** Cui J H, Ma X L, Pu M B, et al. Extraordinary strong optical rotation in weak chiral metasurface[J]. *Opto-Electronic Engineering*, 2020, 47(7): 190052